Dual modes of self-assembly in superstrongly segregated bicomponent triblock copolymer melts

Sebastian Woloszczuk,[1] Kenneth P. Mineart,[2] Richard J. Spontak,[2,3,*] and Michal Banaszak[1,†]

[1]*Faculty of Physics, Adam Mickiewicz University, 61-614 Poznan, Poland*
[2]*Department of Chemical & Biomolecular Engineering, North Carolina State University, Raleigh, North Carolina 27695, USA*
[3]*Department of Materials Science & Engineering, North Carolina State University, Raleigh, North Carolina 27695, USA*

While *ABC* triblock copolymers are known to form a plethora of dual-mode (i.e., order-on-order) nanostructures, bicomponent *ABA* triblock copolymers normally self-assemble into single morphologies at thermodynamic incompatibility levels up to the strong-segregation regime. In this study, we employ on-lattice Monte Carlo simulations to examine the phase behavior of molecularly asymmetric A_1BA_2 copolymers possessing chemically identical endblocks differing significantly in length. In the limit of superstrong segregation, interstitial micelles composed of the minority A_2 endblock are observed to arrange into two-dimensional hexagonal arrays along the midplane of *B*-rich lamellae in compositionally symmetric (50:50 *A*:*B*) copolymers. Simulations performed here establish the coupled molecular-asymmetry and incompatibility conditions under which such micelles form, as well as the temperature dependence of their aggregation number. Beyond an optimal length of the A_2 endblock, the propensity for interstitial micelles to develop decreases, and the likelihood for colocation of both endblocks in the A_1-rich lamellae increases. Interestingly, the strong-segregation theory of Semenov developed to explain the formation of free micelles by diblock copolymers accurately predicts the onset of interstitial micelles confined at nanoscale dimensions between parallel lamellae.

Block copolymers constitute one of the most widely studied classes of soft materials due to their fascinating ability to self-assemble spontaneously into a rich variety of ordered nanoscale morphologies that are of significant fundamental [1,2] and technological [3,4] interest. Tricomponent *ABC* triblock copolymers can exhibit a broad assortment of morphologies [2,5,6], with some displaying unique supramolecular motifs (e.g., the knitting [7] pattern) while many show evidence of dual self-assembly modes (e.g., spheres on or in cylinders or lamellae). Bicomponent *ABA* triblock copolymers, in contrast, generally behave in a similar fashion as their diblock analogs and commonly organize into single morphologies that can be described as $A(B)$ spheres arranged on a face- or body-centered-cubic lattice or $A(B)$ cylinders positioned on a hexagonal lattice in a continuous $B(A)$ matrix, bicontinuous channels, and alternating lamellae [8,9]. These morphologies, retained in physical blends of *ABA* copolymers with macromolecular and/or small-molecule additives [10,11], are largely dictated by interfacial chain packing [12], which can be systematically altered via the chemical composition of the copolymer or the (liquid) crystallinity [13,14] of one or both blocks. Most studies of commercially relevant *ABA* copolymer melts have focused on moderately to strongly segregated systems wherein the chain trajectories can be quantitatively described by existing theoretical frameworks [6,8,9,12,15,16] and the thermodynamic incompatibility, defined as χN (where χ is the Flory-Huggins interaction parameter and N represents the number of repeat units along the copolymer backbone), is typically <100.

At higher values of χN, interfacial tension is expected to dominate over chain packing to regulate morphological development in superstrongly segregated (SSS) block copolymers,

as theoretically described by Nyrkova *et al.* [17] and Semenov *et al.* [18]. Descriptions of such copolymers, however, remain lacking due to one of two practical reasons. At commonly encountered values of χ, the value of N must be large. While high-molecular-weight copolymers have been shown [19] to possess, for example, interesting photonic properties, the likelihood of generating kinetically frozen nonequilibrium or defect-filled morphologies increases with increasing N. Alternatively, at experimentally friendly chain lengths, the needed increase in χ would require the use of constituent species that differ substantially in chemical compatibility. To satisfy this requirement, nonionic SSS block copolymers containing at least one halogenated (usually fluorinated [20–24]) block have been successfully synthesized. Nontraditional morphological features observed in SSS aqueous systems possessing dispersed microdomains include disks [21], lamellar sheets [22], and spindlelike vesicles [24], whereas quadratically perforated lamellae have been identified [20] in SSS copolymer melts. Superstrong segregation can likewise be achieved through the use of charged block copolymers, which has resulted in the formation of toroidal assemblies [25]. In all these investigations of both bicomponent and tricomponent SSS copolymers, a single morphology or a mixture of structurally related morphologies has been reported. We are not aware of any bicomponent copolymer at any segregation level that has exhibited two modes of self-assembly resulting in distinctively different morphological characteristics.

Previous studies [26] of molecularly asymmetric A_1BA_2 triblock copolymers synthesized from a parent diblock copolymer so that $N_{A_1} \neq N_{A_2}$ (where N_{A_1} and N_{A_2} denote the number of repeat units in the A_1 and A_2 blocks, respectively) have helped to elucidate the molecular and property changes accompanying the transformation from an *AB* diblock to a molecularly symmetric *ABA* triblock copolymer (with $N_{A_1} = N_{A_2}$). Recent Monte Carlo (MC) simulations of moderately segregated copolymers have yielded results that

*rich_spontak@ncsu.edu
†mbanasz@amu.edu.pl

quantitatively agree with unexpected experimental findings, most notably a pronounced minimum in the order-disorder transition temperature as N_{A_2} is progressively increased [27]. In this Rapid Communication, we employ the same simulations to investigate the morphological features of SSS A_1BA_2 copolymers and discern how the difference in size between the chemically identical A endblocks affects their ability to self-organize.

Since details of the MC simulations are provided elsewhere [27], an abbreviated overview of the simulation strategy is presented here. The simulations are performed on a face-centered-cubic (fcc) lattice in which the bond length is $\sqrt{2}a$, where a denotes the fcc lattice constant. To ensure that bonds along each copolymer chain are not broken or stretched, we invoke standard periodic boundary conditions. The size of each simulation box is chosen to fit the length of the chain examined, and all lattice sites within the box are completely filled with chain segments (each $\sim$1 kDa) so that the movement of one segment, which defines a single MC step (MCS), necessitates cooperative motion of other segments. The nearest-neighbor interaction energies between i and j segments ($i,j = A$ or B) are given by ε_{ij}, with $\varepsilon_{AA} = \varepsilon_{BB} = 0$ and $\varepsilon_{AB} = \chi kT/7.5$ [28], where k is the Boltzmann constant and T denotes absolute temperature. The A-B interaction parameter is used to define the reduced temperature (T^*) as kT/ε_{AB}. Each simulation commences by equilibrating copolymer chains in the athermal limit so that they become uniformly distributed. From the number of MCSs required for a chain to diffuse a distance on the order of the copolymer gyration radius ($\approx 1.4 \times 10^4$), equilibration is conducted for 5×10^7 MCSs, after which the chains are quenched to a predetermined temperature in the melt and equilibrated for an additional 2×10^6 steps. The following 3×10^6 steps are devoted to data sampling, and each simulation is repeated 6× starting from different initial states to eliminate bias.

To alleviate complications associated with nonequilibration due to long relaxation times (especially at low temperatures), a parallel tempering [29] algorithm has been applied to all simulations performed in this study. According to this protocol, M replicas of each system were simulated for a set of discrete temperatures, $T_1^* < T_2^* < \cdots < T_M^*$, in which the minimum ($T_1^*$) and maximum ($T_M^*$) temperatures were fixed and intermediate temperatures were selected to provide an optimal representation of replicas in temperature space. For a given number of MCSs, adjacent replicas were exchanged in random order according to the probability (p) given by

$$p(T_i^* \leftrightarrow T_{i+1}^*) = \min\{1, \exp[-(\beta_i - \beta_{i+1})(U_{i+1} - U_i)]\}. \tag{1}$$

where $\beta_i = (kT_i^*)^{-1}$ and U_i denotes the potential energy of the replica at T_i^*. If a system was trapped at a low temperature, it was heated to overcome its energy barrier. By using this procedure, improved statistics were generated with fewer MCSs. Here, $M = 36$, with each replica starting in an independent athermal state. After 3000 MCSs, replicas simulated at T_i^* were exchanged with neighboring replicas at T_{i+1}^* according to Eq. (1). The minimum and maximum temperatures were fixed at $T_1^* = 1$ and $T_{36}^* = 10$, respectively, and intermediate temperatures were chosen to follow a geometric distribution.

While the MC approach employed here to simulate A_1BA_2 triblock copolymers has yielded all the conventional morphologies expected in moderately segregated, nonionic bicomponent block copolymers [30], the cross-sectional snapshot displayed in Fig. 1(a) clearly shows the existence of two different modes of self-assembly in a compositionally symmetric (i.e., 50:50 A:B) 46-48-2 copolymer. The long terminal A_1 blocks form the primary morphology composed of lamellar microdomains, whereas the short A_2 endblocks organize into a secondary morphology designated as interstitial micelles, positioned along the midplane of the B-lamella. In this simulation, $\chi N = 480$ and the A_2 fraction (f_{A_2}), where $f_{A_2} = N_{A_2}/(N_{A_1} + N_B + N_{A_2})$, is 0.021. A planar view of the micelles is included in the inset of Fig. 1(a) and reveals that the micelles are arranged on a two-dimensional (2D) hexagonal lattice, resembling a monolayer of block copolymer micelles in ultrathin films [31]. Since the fraction of A repeat units in all the copolymers examined here is ½, the lamellae evident in Fig. 1(a) agree with intuitive expectation. In numerous instances, however, perforated A-lamellae reminiscent of those reported by Burger *et al.* [20] and predicted by Matsen [9] are observed instead, and the corresponding interstitial micelles tend to locate in the B-lamellae at the points of perforation, as shown in Fig. 1(b). These micelles generally appear spherical, unlike the discrete "multiplets" observed in simulations [32] of SSS associating polymers in solution. A schematic diagram of interstitial micelles located between lamellar microdomains is provided in Fig. 1(c) to illustrate a distinguishing characteristic of these micelles: They serve as intermediate physical cross-link sites to connect the primary lamellar morphology across a distance approaching twice the
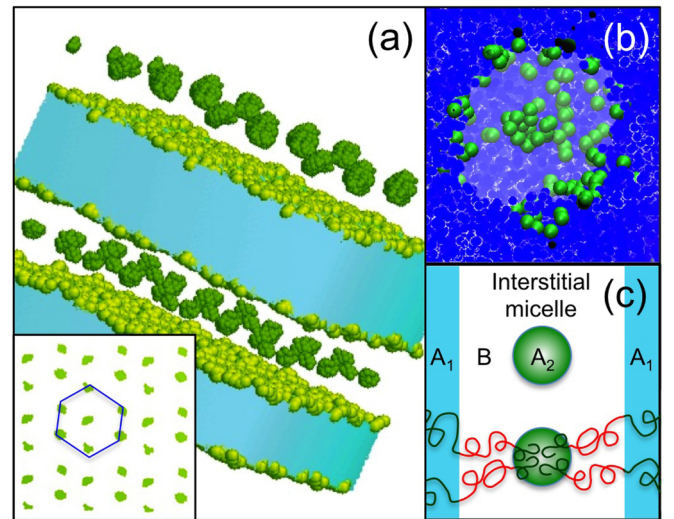

FIG. 1. (Color online) Snapshots of MC simulations of molecularly asymmetric A_1BA_2 triblock copolymers in the SSS regime revealing the existence of interstitial micelles between lamellae [(a) edge view] and perforated lamellae [(b) parallel view through perforation]. Included in (a) is an inset showing the lateral hexagonal packing of the micelles in (a). The schematic illustration in (c) depicts the placement of the blocks (not drawn to scale). In (a)–(c), shades of blue and green refer to A_1 and A_2 features, respectively, whereas red signifies individual B midblocks in (c).

length of the B midblock. In contrast, a midblock bridge in an ABA triblock copolymer network is not capable of extending beyond the distance dictated by the length of its midblock.

Unlike the results presented in Fig. 1, a very short A_2 block in moderately to strongly segregated A_1BA_2 copolymer systems would remain mixed (forming a dangling end) within the B-lamellae, thereby yielding a single lamellar morphology. Formation of the interstitial micelles is therefore a unique manifestation of the conditions examined here. Although theoretical frameworks predicting the coexistence of two different morphologies in a molten SSS copolymer are lacking, the theory proposed by Semenov *et al.* [18] describes the thermodynamics of micelles in the SSS regime. Since morphological development is largely governed by interfacial tension in their model, they identify a critical interfacial tension (γ_c) that signifies the onset of superstrong segregation, as well as the micellar aggregation number (Q) that ensues when $\gamma > \gamma_c$. The functional forms of γ_c and Q derived for spherical micelles, however, assume that the coronal free energy can be written in the same fashion as that in the strong-segregation limit. Their theory also addresses the formation of SSS nonspherical micelles, including disks. Since $\gamma \sim \chi^{1/2}$ and $\chi \sim 1/T$, their theory suggests that SSS micelles should

become less stable with increasing temperature. We explore this behavior for two systems possessing different values of N in Fig. 2, which shows the effect of temperature on chain trajectories by displaying the fractions of A_2 blocks involved in forming interstitial micelles (υ_M), conventional bridges and loops wherein both endblocks colocate in A-lamellae (υ_L), and nonassociated dangling ends (υ_D) as functions of T^*. These fractions are subject to the constraint that $\upsilon_M + \upsilon_L + \upsilon_D = 1$ since completely unsegregated chains are expected to be negligible in this regime.

In the first system examined [Figs. 2(a)–2(c)], the A_1BA_2 copolymer is designated (40-x)-40-x, where x is varied from 1 to 4. When $x = 1$ [Fig. 2(a)] at the lowest temperature considered ($T^* = 1.0$), the system consists primarily of double-anchored chains with $\upsilon_L = 0.88$. As T^* is increased slightly (to ≈ 1.1), υ_M reaches a maximum (at 0.23) and then drops to zero as T^* is increased further. In contrast, υ_L generally decreases, while υ_D increases, up to $T^* \approx 7.7$. Above this temperature, υ_L shows signs of increasing while υ_D starts to decline. As the short terminal block is lengthened [$x = 2$ in Fig. 2(b)], the system displays slight evidence of micelle-forming bridges over a finite T^* range extending from about 1.9 to 3.3 while υ_L remains above 0.90. An increase
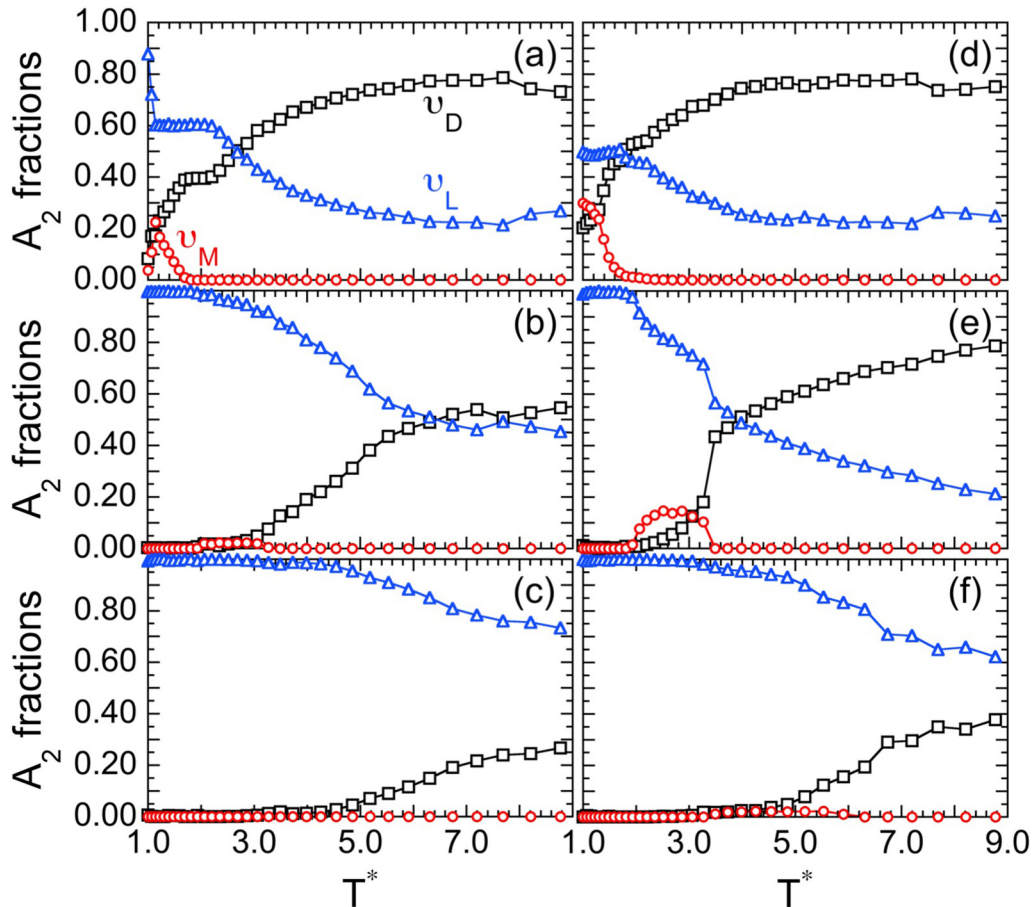

FIG. 2. (Color online) Values of the A_2 block fractions extracted from MC simulations of SSS A_1BA_2 triblock copolymers—(a) 39-40-1, (b) 38-40-2, (c) 37-40-3, (d) 47-48-1, (e) 46-48-2, and (f) 45-48-3—provided as functions of reduced temperature (T^*). The fractions shown include micelle-forming bridges (υ_M, red circles), double-anchored chains (υ_L, blue triangles), and dangling ends (υ_D, black squares). The solid lines connect the data, and the sizes of the simulation boxes employed here are (a)–(c) $80 \times 40 \times 40$ and (d)–(f) $96 \times 48 \times 48$ to explore size effects.

in temperature promotes a continued increase in υ_D and a corresponding decrease in υ_L until the two fractions cross and then become nearly temperature-independent. When $x = 3$ [Fig. 2(c)] and $x = 4$ (not shown), the systems appear similar and are composed entirely of double-anchored chains with no micelle-forming bridges or dangling ends at low T^*. The distinguishing feature between the two is the value of T^* at which υ_L decreases (and υ_D increases) shifts to higher temperatures (2.9 when $x = 3$ and 4.3 when $x = 4$). Comparable results are observed in the second copolymer, designated (48-x)-48-x, in Figs. 2(d)–2(f). One noticeable difference is that the fraction of micelle-forming bridges remains nonzero over a finite temperature range for $x = 1$–3 (but reduces to zero for all T^* when $x = 4$). The results displayed in Fig. 2 indicate that fewer chains form interstitial micelles, and the micelles ultimately become unstable, at elevated temperatures. In addition, while the copolymer systems initially favor double-anchored chains at low T^* as x is increased, an increase in kT eventually generates dangling ends due to the corresponding reduction in incompatibility between A and B segments.

Average values of Q measured from several simulations are provided as a function of T^* in Fig. 3 and confirm that the interstitial micelles in Fig. 1 generally develop at low T^* (high χN) for copolymers with relatively small A_2 blocks. In complementary dissipative particle dynamics (DPD) simulations performed under the conditions described elsewhere [30], the perforated lamellae and interstitial micelles generated in MC simulations are also observed. While Q consistently remains between 10 and 20 in the DPD simulations, Fig. 3 reveals that a slight increase in the size of the A_2 block can promote a significant increase in Q, along with enhanced thermal stability. If the A_2 block becomes too large, however, then micelles do not form. This observation suggests that, for a given copolymer incompatibility, interstitial micelles develop over a relatively narrow range in f_{A_2}. To explore this relationship, we plot the corresponding upper and lower stability limits of interstitial micelles as discerned from a compilation of simulations in Fig. 4. At χN below the lower
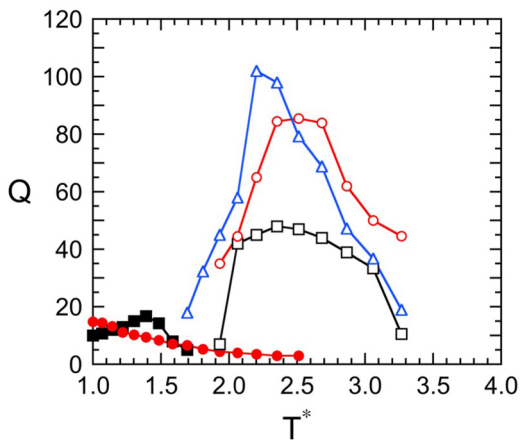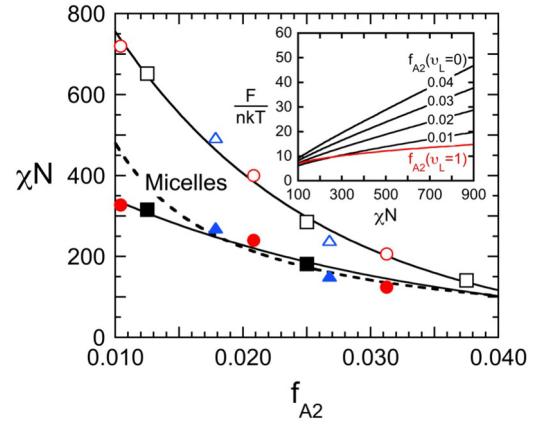

FIG. 4. (Color online) The upper and lower stability limits (open and solid circles, respectively) for interstitial micelles in A_1BA_2 triblock copolymers with short A_2 blocks compiled from MC simulation results for copolymers varying in chain length (N): 80 (black squares), 96 (red circles), and 112 (blue triangles). The solid lines are guides for the eye, and the dashed line corresponds to Eq. (3) in the text (evaluated under the specified conditions). The inset displays the dimensionless free energy as a function of χN from Eq. (2) for dangling ends ($\upsilon_L = 0$, black curves) and double-anchored chains ($\upsilon_L = 1$, red curve) at different f_{A_2} (labeled).

stability limit, not all the A_2 blocks form double-anchored chains, in which case dangling ends exist (cf. Fig. 2). When χN lies above the upper stability limit, every A_2 block is sufficiently incompatible with the B midblock to microphase-separate and colocate with the A_1 blocks in the A-lamellae. The range over which the micelles are stable for a given χN value is not large ($<1\%$). Intended to serve as a guide for the eye, each of the solid lines included in Fig. 4 obeys a scaling relationship of the form $f_{A_2} \sim \ln(\chi N)$. By setting equal the regression equations for the two limits, we estimate that the stability regime for interstitial micelles terminates in the vicinity of $f_{A_2} \approx 0.046$ and $\chi N \approx 81$.

Although a rigorous theoretical treatment of the present copolymer system is beyond the scope of this Rapid Communication, we first consider the free energy of lamellae-forming asymmetric triblock copolymers in the strong-segregation theory proposed by Matsen [9]. The dimensionless free energy (F/nkT, where n is the number of chains) evaluated at the equilibrium lamellar period is

$$\frac{F}{nkT} = \frac{3}{4}\left[\frac{\pi^2 h(\upsilon_L)\chi N}{3}\right]^{1/3} + \chi N f_{A_2}(1 - \upsilon_L), \quad (2)$$

where $h(\upsilon_L) = (1 + 2f_{A_2} - f_A)(1 + 3\upsilon_L^2) - (2f_{A_2} - f_A)$, and υ_L is assumed in this framework to equal $1 - \upsilon_D$. The inset in Fig. 4 shows free-energy predictions from Eq. (2) for the limiting case of dangling ends only ($\upsilon_L = 0$) at several values of f_{A_2}. As expected, the free energy increases with an increase in N_{A_2}, confirming that the existence of long dangling A_2 endblocks in B-lamellae becomes increasingly less energetically favorable. One way to lower the free energy in this limit is for both endblocks to colocate within A-lamellae, which at the opposite extreme corresponds to the case of $\upsilon_L = 1$ included in the inset. (While results for $f_{A_2} = 0.04$ are shown, predictions for lower f_{A_2} are

FIG. 3. (Color online) Dependence of the micelle aggregation number (Q) on T^* for copolymers designated as (40-x)-40-x (black squares), (48-x)-48-x (red circles), and (56-x)-56-x (blue triangles) for the cases of $x = 1$ (solid symbols) and $x = 2$ (open symbols). The solid lines connect the data.

indistinguishable at the scale shown.) The simulations reported here indicate that another way to reduce the free energy not considered in Eq. (2) is by the formation of interstitial micelles. Although Eq. (2) can, in principle, be extended into three dimensions to account for the presence of interstitial micelles, we consider an alternative means of analyzing the data in Fig. 4. According to Semenov [33], the condition signaling the formation of a single free micelle by AB diblock copolymer molecules in the SS limit is satisfied by

$$\alpha = -\ln f_{A_2} + \frac{1}{2}\ln \alpha + 2.06\alpha^{1/3}, \qquad (3)$$

where $\alpha = \chi N f_{A_2}$, Since each A_1 endblock is restricted to an A-lamella in the present scenario, only the A_2 endblock and B midblock of each copolymer molecule participate in micelle formation. In this case, we treat these blocks as the equivalent of a tethered A_2B diblock molecule and correspondingly calculate α in Eq. (3) at $f'_{A_s} = N_{A_2}/(N_{A_2} + N_B)$. The resultant predictions displayed in Fig. 4 quantitatively match the MC simulations at $\chi N < 300$ without any adjustable parameters. Such favorable agreement implies that, despite being (i) constrained between lamellae (which behave as soft parallel surfaces [34]), (ii) tethered at one chain end, and (iii) surrounded by double-anchored midblocks, the interstitial micelles reported in this study form as if they were free micelles in the bulk.

While bicomponent ABA triblock copolymers normally order into single morphologies, numerous experimental studies [35,36] have demonstrated that coexisting morphologies frequently develop during solvent casting. Recent evidence [37] acquired from melt-spun bicomponent fibers confirms that dual-mode nanostructures (e.g., tubes containing centerline micelles) can likewise form in solvent-free systems. The MC simulations presented here establish that molecularly asymmetric triblock copolymers can exhibit two different modes of self-assembly near equilibrium in the SSS regime: lamellae and interstitial micelles (in some cases positioned on a 2D hexagonal lattice). These results have been validated over a wide range of conditions and have likewise been confirmed by DPD simulations. Detailed analysis of the MC simulations indicates that the population of micelle-forming chains, as well as the micelle aggregation number, is sensitive to copolymer composition and incompatibility. Using molecularly asymmetric triblock copolymers to decorate a primary morphology (e.g., the lamellae observed here, or spheres or cylinders at other copolymer compositions) with interstitial micelles opens a different route to generating two concurrent and independent levels of spatially modulated nanostructures in bicomponent block copolymers, and provides an opportunity to explore variations in the phase behavior and properties (due, for instance, to enhanced physically stabilized molecular networks) of designer multiblock copolymers [38] in the largely overlooked SSS regime.

[1] I. W. Hamley, *The Physics of Block Copolymers* (Oxford University Press, New York, 1998).

[2] F. S. Bates and G. H. Fredrickson, Phys. Today **52**(2), 32 (1999).

[3] C. Park, J. Yoon, and E. L. Thomas, Polymer **44**, 6725 (2003).

[4] M. Lazzari, G. Liu, and S. Lecommandoux, *Block Copolymers in Nanoscience* (Wiley-VCH, Weinheim, 2006).

[5] V. Abetz, in *Encyclopedia of Polymer Science and Technology*, 3rd ed., edited by J. I. Kroschwitz (Wiley, Hoboken, NJ, 2003), Vol. 1, pp.482–523.

[6] Z. J. Guo, G. J. Zhang, F. Qiu, H. D. Zhang, Y. L. Yang, and A.-C. Shi, Phys. Rev. Lett. **101**, 028301 (2008).

[7] V. Abetz and P. F. W. Simon, Adv. Polym. Sci. **189**, 125 (2005).

[8] M. W. Matsen and R. B. Thompson, J. Chem. Phys. **111**, 7139 (1999).

[9] M. W. Matsen, J. Chem. Phys. **113**, 5539 (2000).

[10] P. Alexandridis, U. Olsson, and B. Lindman, Langmuir **14**, 2627 (1998).

[11] A. S. Krishnan, S. D. Smith, and R. J. Spontak, Macromolecules **45**, 6056 (2012).

[12] M. W. Matsen and F. S. Bates, J. Chem. Phys. **29**, 7641 (1996).

[13] J. T. Chen, E. L. Thomas, C. K. Ober, and G. P. Mao, Science **273**, 343 (1996).

[14] J. Raez, I. Manners, and M. A. Winnik, J. Am. Chem. Soc. **124**, 10381 (2002).

[15] M. W. Matsen and M. Schick, Macromolecules **27**, 187 (1994).

[16] F. Drolet and G. H. Fredrickson, Phys. Rev. Lett. **83**, 4317 (1999).

[17] I. A. Nyrkova, A. R. Khokhlov, and M. Doi, Macromolecules **26**, 3601 (1993).

[18] A. N. Semenov, I. A. Nyrkova, and A. R. Khokhlov, Macromolecules **28**, 7491 (1995).

[19] E. P. Chan, J. J. Walish, A. M. Urbas, and E. L. Thomas, Adv. Mater. **25**, 3934 (2013).

[20] C. Burger, M. A. Micha, S. Oestreich, S. Förster, and M. Antonietti, Europhys. Lett. **42**, 425 (1998).

[21] T. P. Lodge, M. A. Hillmyer, Z. L. Zhou, and Y. Talmon, Macromolecules **37**, 6680 (2004).

[22] R. R. Taribagil, M. A. Hillmyer, and T. P. Lodge, Macromolecules **43**, 5396 (2010).

[23] S. Qin, H. Li, W. Z. Yuan, and Y. M. Zhang, Polymer **52**, 1191 (2011).

[24] J.-N. Deng, W.-B. Wang, Z.-H. Zheng, X.-B. Ding, and Y.-X. Peng, Chin. J. Polym. Sci. **32**, 817 (2014).

[25] D. J. Pochan, Z. Y. Chen, H. G. Cui, K. Hales, K. Qi, and K. L. Wooley, Science **306**, 94 (2004).

[26] M. W. Hamersky, S. D. Smith, A. O. Gozen, and R. J. Spontak, Phys. Rev. Lett. **95**, 168306 (2005).

[27] S. Woloszczuk, M. Banaszak, and R. J. Spontak, J. Polym. Sci. B **51**, 343 (2013).

[28] D. C. Morse and J. K. Chung, J. Chem. Phys. **130**, 224901 (2009).

[29] T. M. Beardsley and M. W. Matsen, Eur. Phys. J. E **32**, 255 (2009).

[30] S. S. Tallury, K. P. Mineart, S. Woloszczuk, D. N. Williams, R. B. Thompson, M. A. Pasquinelli, M. Banaszak, and R. J. Spontak, J. Chem. Phys. **141**, 121103 (2014).

[31] G. E. Stein, E. J. Kramer, X. F. Li, and J. Wang, Macromolecules **40**, 2453 (2007).

[32] P. G. Khalatur, A. R. Khokhlov, I. A. Nyrkova, and A. N. Semenov, Macromol. Theory Simul. **5**, 713 (1996).

[33] A. N. Semenov, Sov. Phys. JETP **61**, 733 (1985).

[34] A. Cavallo, M. Müller, and K. Binder, Macromolecules **41**, 4937 (2008).

[35] D. Bendejacq, V. Ponsinet, M. Joanicot, Y. L. Loo, and R. A. Register, Macromolecules **35**, 6645 (2002).

[36] K. P. Mineart, X. Jiang, H. Jinnai, A. Takahara, and R. J. Spontak, Macromol. Rapid Commun., doi:10.1002/marc.201400627.

[37] S. A. Arvidson, K. E. Roskov, J. J. Pate, R. J. Spontak, S. A. Khan, and R. E. Gorga, Macromolecules **45**, 913 (2012).

[38] F. S. Bates, M. A. Hillmyer, T. P. Lodge, C. M. Bates, K. T. Delaney, and G. H. Fredrickson, Science **336**, 434 (2012).